JACS
JOURNAL OF THE AMERICAN CHEMICAL SOCIETY

Article

pubs.acs.org/JACS

# Sequential Proton Coupled Electron Transfer (PCET): Dynamics Observed over 8 Orders of Magnitude in Time

Luke MacAleese,*[,†] Sylvain Hermelin,[‡] Krystel El Hage,[§] Pierre Chouzenoux,[†] Alexander Kulesza,[†] Rodolphe Antoine,[†] Luigi Bonacina,[‡] Markus Meuwly,[§] Jean-Pierre Wolf,[‡] and Philippe Dugourd[†]

[†]Institut Lumière Matière, UMR5306 Université Claude Bernard Lyon1-CNRS, Université de Lyon 69622 Villeurbanne cedex, France
[‡]Group of Applied Physics (GAP) Biophotonics, Université de Genève, Chemin de Pinchat 22, CH-1211 Geneva, Switzerland
[§]Department of Chemistry, University of Basel, Klingelbergstr 80, CH-4056 Basel, Switzerland

Supporting Information

**ABSTRACT:** Charge transfer mechanisms lay at the heart of chemistry and biochemistry. Proton coupled electron transfers (PCET) are central in biological processes such as photosynthesis and in the respiratory chain, where they mediate long-range charge transfers. These mechanisms are normally difficult to harness experimentally due to the intrinsic complexity of the associated biological systems. Metal-peptide cations experience both electron and proton transfers upon photoexcitation, proving an amenable model system to study PCET. We report on a time-resolved experiment designed to follow this dual charge transfer kinetics in $[HG_3W+Ag]^+$ (H = histidine, G = glycine, W = tryptophan) on time scales ranging from femtoseconds to milliseconds. While electron transfer completes in less than 4 ps, it triggers a proton transfer lasting over hundreds of microseconds. Molecular dynamics simulations show that conformational dynamic plays an important role in slowing down this reaction. This combined experimental and computational approach provides a view of PCET as a single phenomenon despite its very wide time-domain span.

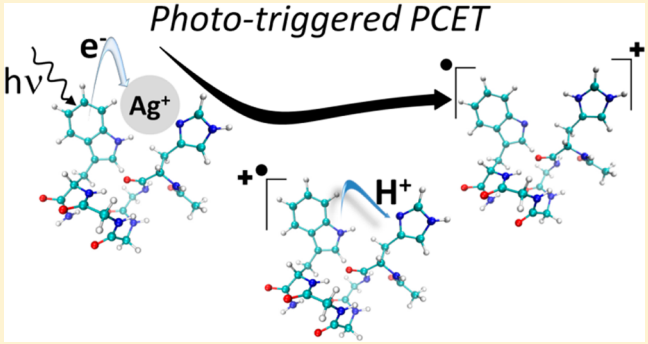


## INTRODUCTION

Proton-coupled electron transfer (PCET) reactions are ubiquitous in biology and involve both concerted and sequential mechanisms.[1−3] They enable energy conversion and storage in photosynthesis[4] and in the respiratory chain,[5,6] mediate charge transfers,[7] are involved in DNA repair,[7] and provide low energy paths in enzymatic reactions (particularly around metallic centers[8,9]). Theoretical[2] and experimental approaches[8,10−15] have been proposed to address the steady state energetics and kinetics of PCET in different environmental conditions. However, kinetics remain difficult to access directly. Various time-resolved approaches have been applied to investigate in solution the dynamics of such systems,[7,14,16−21] ranging from stopped-flow experiments[9] to pump−probe experiments with ultrafast Raman spectroscopy.[20,21] However, those studies are limited to time spans within a few orders of magnitude. Gas-phase time-resolved photoexcitation dynamics and relaxation in biomolecules have been proposed but are also restricted to either ultrafast[22−27] or slow[28] processes.

We selected $[HG_3W+Ag]^+$ (H = histidine, G = glycine, W = tryptophan) as a model system to study the full sequence of a photoinduced PCET reaction in the gas phase. Metallic centers are commonly involved in PCET processes, as well as in catalytic cycles in general. This is due to their ability to change oxidation state via metal to ligand charge transfers (MLCT) with somewhat low energy demand. Their role in photosynthesis is central and introduces a family of excited-state PCET reactions. Here, we study the complete dynamics of the sequential PCET in $[HG_3W+Ag]^+$ by pump−probe experiments, transition state calculations and molecular dynamics (MD) simulations. A radical peptide cation[29−33] is generated by photoexcitation. Steady state studies[32,34] suggest that in the formed radical peptide $[HG_3W]^{\bullet+}$, the charge and radical are initially localized on the tryptophan, and that a proton is sequentially transferred from the tryptophan to the histidine (Figure 1). The experimental study covers 8 orders of magnitude in time and shows that the 4 ps electron transfer induces a proton transfer hundreds of microseconds later. Molecular dynamics simulations reveal that conformational changes of the peptide play a key role in the proton transfer.

## RESULTS

A 266 nm laser pump pulse irradiates the metal-peptide complex $[HG_3W+Ag]^+$ and excites specifically a $\pi-\pi^*$ transition of tryptophan, leading to the observation of intense fragments without silver (Figure S1). This is interpreted as a crossing between the initially excited $\pi-\pi^*$ state on tryptophan

**Received:** December 2, 2015
**Published:** March 14, 2016





DOI: 10.1021/jacs.5b12587
J. Am. Chem. Soc. 2016, 138, 4401−4407

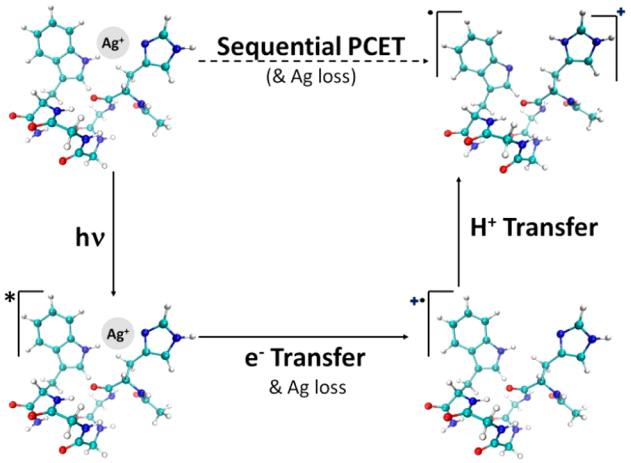


**Figure 1.** Schematic representation of PCET dynamics in $[HG_3W+Ag]^+$ metal–peptide complexes. Irradiation at 266 nm initiates an electron transfer from tryptophan to $Ag^+$, leading to the loss of Ag. The electron transfer is followed by a proton transfer from tryptophan to histidine with formation of a distonic ion. The peptide structures are schemes and do not correspond to calculated structures.

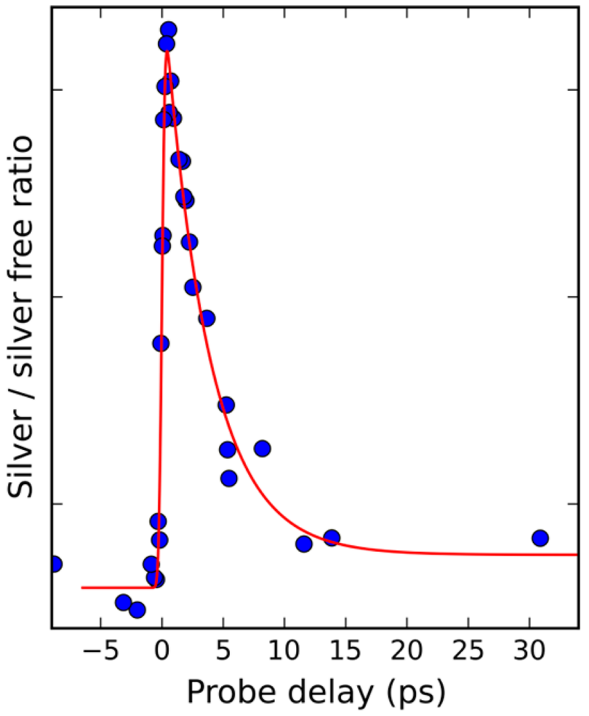


**Figure 2.** Evolution as a function of the pump–probe delay of the ratio between silver-containing vs silver-free fragment ions. Experimental data (blue circles) is fitted (red line) with a monoexponential decay response convoluted to a Gaussian pulse shape corresponding to the cross-correlation of the pump and probe pulses (fwhm 470 fs). The fit provides a time constant of 3.5 ps for the decay.

(or a secondary electronically excited state accessed from the $\pi-\pi^*$ state) and a dissociative charge transfer (electron transfer—ET) state. In this ET state, silver is neutral and the positive charge is on the now radical peptide. The metastable complex dissociates to launch the radical peptide cation $[HG_3W]^{\bullet+}$. Previous studies indicate that the transferred electron originates from tryptophan.[32] Thus, the resulting radical peptide cation has initially both charge and radical colocalized on tryptophan ($W^{\bullet+}$). However, a proton transfer (PT) from tryptophan to histidine is expected when comparing the proton affinity (PA) reported for neutral histidine (231.5 kcal/mol[35]) and for the indolyl radical (227.6 kcal/mol[36])—radical tryptophan's side chain. This PT is evidenced by the observation of the optical signature of neutral radical tryptophan[34] in the steady state optical spectrum of $[HG_3W]^{\bullet+}$. It leads to the distonic ion with charge ($His^+$) and radical ($W^{\bullet}$) on separate sites. This multistep dynamics was monitored by irradiating the system with a visible probe pulse, at varying delays, which induces extra photofragmentation of either the metal complex or of the pump-associated fragments. Details of ET and PT analyses are given in the following sections.

**Electron Transfer from Peptide to Metal.** The electron transfer from the peptide to the metal was followed by analyzing the ratio of silver-containing (S) to silver-free (SF) ions. The probe pulse alone does not induce photofragmentation (Figure S1) and therefore, for negative delays, the effect of the pump pulse only is observed. At $t = 0$, the S/SF ratio significantly increases. This rapid increase in silver containing fragments (which is experimentally time limited by the pump–probe temporal convolution of our measurement, around 400 fs) is due to fragmentation induced by the probe pulse prior to ET toward silver. It confirms that the positive charge is initially localized on the silver atom in the metal-peptide complex. For positive delays, the S/SF ratio decreases showing that the positive charge is transferred toward the peptide at longer times. At very long delays the low S/SF ratio (Figure 2) goes back to S/SF level induced by the pump only. This demonstrates the transfer of an electron from the peptide to the silver atom, which is completed in 3.5 ps and leads to the formation of a radical tryptophan cation ($W^{\bullet+}$).

**Optical Spectroscopy of $W^{\bullet+}$ vs $W^{\bullet}$.** The optical properties of the two structures ($W^{\bullet+}$ and $W^{\bullet}$) adopted by the radical cation $[HG_3W]^{\bullet+}$ were assessed by steady state ion spectroscopy. $[G_3W]^{\bullet+}$ is used as a model for $W^{\bullet+}$ where both the radical and ionized sites are localized on tryptophan. $[HG_3W]^{\bullet+}$ and $[G_3W]^{\bullet+}$ were generated by collision induced dissociation (CID) of a complex between the neutral peptide and a liganded copper (Cu-terpyridine).[29−31] Cations were then mass selected and isolated in the ion trap and their photofragmentation yield (FY) spectra measured (Figure 3). The time scale of the radical peptides preparation is such (~200 ms) that they have relaxed to their most stable structure before their optical properties are probed. $[HG_3W]^{\bullet+}$ is then assumed in the $^+HG_3W^{\bullet}$ form, deprotonated at indoleNH as confirmed by comparison with TD-DFT spectra (Figure S10). Figure 3 displays the spectra of both radicals recorded simultaneously, under identical instrumental conditions. As a consequence spectra can be directly compared not only in terms of band positions but more importantly in terms of relative fragmentation yields (FY). Figure 3 shows that the $W^{\bullet+}$ species display a 7-fold more intense FY than the $W^{\bullet}$ species, with a band strongly red-shifted from 480 to 550 nm. For both species the band is broad (fwhm ~100 nm) and the FY of the $W^{\bullet+}$ species is always higher than that of the $W^{\bullet}$ species, even at its maximum at 480 nm. As a consequence, in $[HG_3W]^{\bullet+}$, a PT phenomenon from the tryptophan to the histidine is expected to induce a significant decrease in FY at 580 nm as a function of time.


DOI: 10.1021/jacs.5b12587
J. Am. Chem. Soc. 2016, 138, 4401−4407

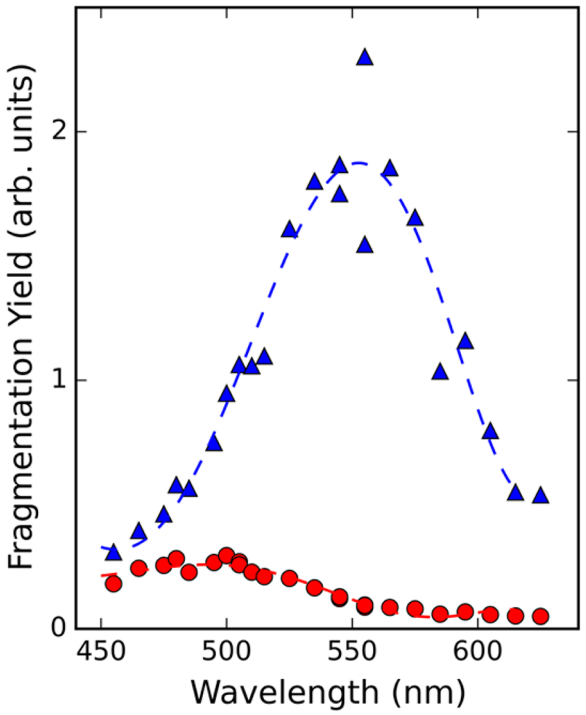


**Figure 3.** Steady state optical action spectra (FY) in the visible range for isolated gas-phase radical peptides $[G_3W]^{\bullet+}$ (blue triangles) and $[HG_3W]^{\bullet+}$ (red circles). Dashed lines are a guide for the eyes.

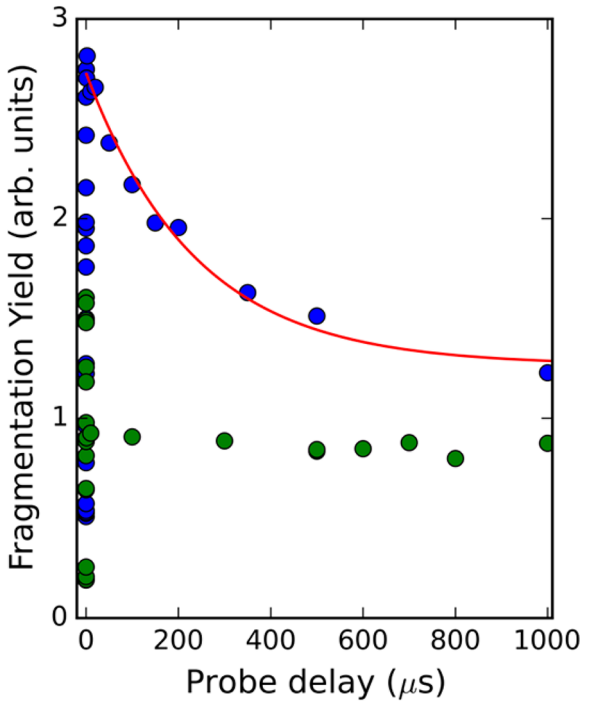


**Figure 4.** Evolution of $[HG_3W]^{\bullet+}$ radical peptide fragmentation yield as a function of the pump–probe delay at two different probe wavelengths. The amplitude decay observed in experimental data at 580 nm (blue circles) for positive delays is fitted with a monoexponential decay function (red line) that provides a time constant of ~250 $\mu$s.

**Proton Transfer from $W^{\bullet+}$ to H: Transition from $W^{\bullet+}$ to $W^{\bullet}$.** The PT dynamics after the initial electron transfer and silver loss was followed using the same pump–probe technique as for the ET, but on much longer time scales. Fragments of the radical peptide cation (silver-free ions) were monitored as a function of delay. The pump–probe scan with the femtosecond laser shows that the FY remains high and constant up to 500 ps (Figure S3). The pump–probe delay range was therefore increased up to 30 ms using two nanosecond laser sources and electronic temporal synchronization. Figure 4 displays the radical peptide FY values measured with the nanosecond setup for delays up to 1 ms. FY was probed at different wavelengths. When the probe is set at 580 nm, FY exhibits a decay. According to the FY difference observed in Figure 3 at 580 nm, this decay in FY amplitude is in agreement with a PT occurring from radical tryptophan to histidine. Comparatively, FY displays no decay when the probe is set at 470 nm. This is consistent with the transition from $HG_3W^{\bullet+}$ to $^{+}HG_3W^{\bullet}$ as the two species display almost identical FY at that wavelength (Figure 3). The decay at 580 nm could be fitted with an exponential decay with a time constant of 250 $\mu$s. The proton transfer time scale of a few hundreds of microseconds is confirmed by measurements at other probe wavelengths (Figure S4) and is surprisingly similar on the deuterated species (Figure S8).

**Atomistic Simulations and Computations.** Molecular dynamics simulations were performed from three different initial structures of the radical peptide: an extended structure, and the two compact conformations obtained from DFT-optimized structures of the $[Ag+HG_3W]^{+}$ complex[33] (Figure S7). In each case, the formation dynamics of the "PT reactive" H-bond between the indoleNH of tryptophan and the imidazoleN of histidine is followed. Starting from the extended structure, the probability to form this H-bond (peak at 1.9 Å) is very high (0.87) and occurs on the nanosecond time scale (Figures 5A and S6). However, starting from the compact conformation, this probability decreases to 0.53 and 0.18 (Figure 5B/C) depending on the starting structure. In order to corroborate this result, MD simulations starting from the compact structure in Figure S7D were extended to an overall time of 8 $\mu$s, in the case of the most stable compact

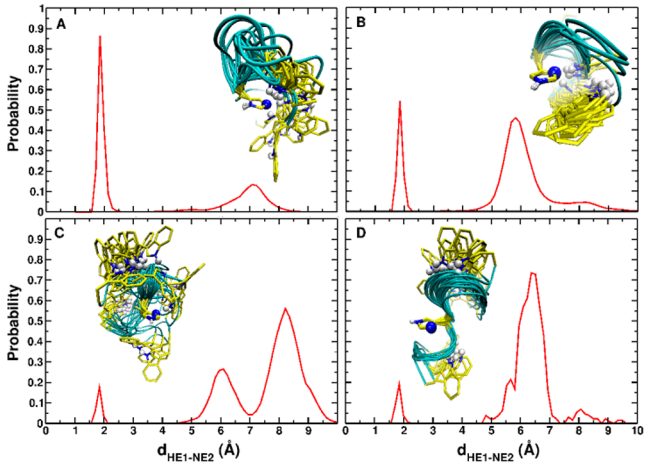


**Figure 5.** IndoleNH–imidazoleN distance distribution in $HG_3W^{\bullet+}$ over 50 independent runs of 10 ns each, starting from an extended structure (A) and two compact structures (B and C) obtained from the $[HG_3W+Ag]^{+}$ complex. (D) Same but over 8 independent runs of 1 $\mu$s each, starting from structures in C. Insets show superpositions of structures from MD trajectories.



DOI: 10.1021/jacs.5b12587
J. Am. Chem. Soc. 2016, 138, 4401–4407

conformation, with no increase of those probabilities (Figure 5D).

The free energy barrier for a direct proton transfer from tryptophan to histidine along the reactive H-bond is 53.4 kJ/mol (obtained after transition state optimization, see Methods). For this indoleNH to imidazoleN PT pathway, a kinetic isotope effect (KIE) ~3.6 at 298 K, and 2.6 at 400 K, was calculated using the zero-point energies (ZPE) at the B3LYP/6-31G* level of theory (see Methods).

## DISCUSSION

It was shown experimentally that electron transfer occurs within 3.5 ps after photon excitation, while proton transfer takes over a few hundred microseconds, i.e., is about 8 orders of magnitude slower.

The overall dynamics after the initial photoexcitation at 266 nm, schematically presented in Figure 1, is inferred to be as follows. The initial electron transfer results from a crossing between the excited $\pi-\pi^*$ state and the dissociative charge-transfer state as observed for protonated systems.[37,38] Previous work reported shorter lifetimes of 100−400 fs[39,40] for similar protonated tryptophan $\pi-\pi^*$ states. The 3.5 ps time scale measured for this ET is nevertheless consistent with excited state lifetimes observed in silver−DNA basis complexes[41] (>5 ps vs 85 fs for protonated complexes) where it was associated with hindered out-of-plane vibrations resulting in less efficient internal conversion from $\pi-\pi^*$ to ground state. When back-conversion to the ground state is hindered, lifetime is increased and transition to other states (in particular charge transfer states) is favored. This is consistent with the observation of Ag loss as the main photofragmentation pathway, resulting in the charged peptide where both the charge and radical character are localized on the tryptophan residue.

At that point, after photon absorption, ET and dissociation of neutral Ag from the radical peptide, a rough upper estimate indicates that the peptide temperature is ~400 K (this value accounts for the absorption of a photon at 266 nm, the loss of the $HG_3W-Ag^+$ binding energy[33] and the ionization energy difference between Ag and $HG_3W$) . Starting from this "hot" $W^{\bullet+}$ structure, PT involves a 53.4 kJ/mol free energy barrier once an adequate "reactive" conformation has been reached. According to transition state theory (TST), and taking into account the accuracy of the method (±10 kJ/mol for energetics of gas-phase reactions[42]), such a barrier height is associated with time constants in the range of a few microseconds, suggesting that it is not the rate-limiting step. Additionally, the experimentally measured PT time scale is identical (a few hundred microseconds) for both deuterated and nondeuterated species (Figure S8), which yields a primary kinetic isotope effect (KIE) ~1. The possibility of PT involving a non-substituted hydrogen was ruled out by two observations. First, the steady state spectrum of the peptide radical after 200 ms indicates that the transferred proton leaves from indoleNH (Figures 3 and S10). Second, NMR $^1H$ spectra confirm that the indoleNH on tryptophan is rapidly substituted with deuterium together with all labile hydrogens (Figure S9). Thus, since the expected KIE associated with the PT activation barrier in the system at 400 K is calculated at 2.6, i.e. well above the observed KIE ≈ 1, PT cannot be the rate limiting step.

Molecular dynamics simulations show that the rate of formation of a PT-reactive structure (H-bond between indoleNH on tryptophan and imidazoleN on histidine) strongly depends on the initial peptide structure (Figure 5). In particular, while this rate is in the nanosecond range when starting from an extended conformation (Figures 5A and S6), it is considerably longer when starting from compact peptide conformations as in the initial metal complex (Figure 5B−D). In this complex, peptide conformation is stabilized but constrained by the presence of $Ag^+$. In the metal-containing complex, the Trp side chain is oriented away from His, and indoleNH forms favorable H-bonds with backbone carbonyls on glycine residues (Figure S7A, D). After ET and neutral Ag loss, side chain reorientation is hindered because several O- and N atoms are already engaged in H-bonds "locking" the peptide conformation (Figure S7B, C, E, F). The network of pre-existing H-bonds involving the backbone hinders the formation of the PT-reactive H-bond which is considerably slowed-down: on a time scale of 8 $\mu$s, no formation of a PT-reactive structure was observed (Figure 5D). This, together with the observed KIE ≈ 1, suggests that the structural rearrangement is a slow process and is rate-limiting.[43,44]

## CONCLUSION

In conclusion, we observed a direct proton transfer from radical tryptophan cation to histidine, with a time scale of a few hundred microseconds. While the measured PT time scale is longer than what can be observed in highly coupled organic systems such as pairs of DNA bases[45] or porphyrins,[12,46,47] it is in good agreement with proton translocation rates in solution and in particular inside protein.[48] Here, gas phase experiments allowed to observe the proton transfer triggered by a 3.5 ps electron transfer as a sequential photoinduced PCET phenomenon, despite its very wide time-domain span. The conformational dynamics play a crucial role in the overall proton transfer dynamics, as shown by atomistic simulations; this conclusion can probably be generalized to more complex biological systems.

## METHODS

**Chemistry, Sample Preparation.** Silver nitrate from Sigma was used in water solution with concentration 25 mM. CopperII-terpyridine was synthesized in the lab[49] and solubilized in water. Solid peptides $HG_3W$ and $G_3W$, both N-acetylated and C-amidated, were bought from Genecust, desalted and with purity >70%. 10 $\mu$M solutions of peptide with small excess of metal (Ag or CuTerpyridine) were prepared in water/methanol (1:1), and electrosprayed as is in the mass spectrometer. Deuteration of the peptide was performed by solubilizing the crystals in $D_2O$ and performing ESI in $D_2O$/methanol-1D.

**Mass Spectrometry.** A commercial dual linear ion trap (LTQ-VELOS, ThermoScientific) was used to generate, mass select, and trap ions in a first, high pressure (5 mTorr) ion trap, for a controlled duration. During ion trapping, ions can be activated and fragmented by collisions (CID) or photons. Fragment ions are transmitted to a second ion trap, with low pressure, where they are mass analyzed. A fused silica window (3 mm thick, 1 in. diameter) is positioned at the back end of the instrument and allows for the introduction of laser beams in the UV−visible range along the ion trap axis. 1−2 mm diameter circular openings in trapping-electrodes enable on axis laser interaction beam with ions in the first ion trap. In order to optimize laser transmission through the second ion trap, the central hole of the electrode closest to the fused silica window was enlarged to 5 mm in diameter. Electrospray ionization (ESI) conditions are typically spray voltage 5 kV, sample flow 3 $\mu$L/min. Ion accumulation times are <10 ms, and signal levels after ion selection are above $10^3-10^4$. 1000 individual mass spectra are accumulated at each scanned value (laser wavelength or pump−probe delay).



DOI: 10.1021/jacs.5b12587
J. Am. Chem. Soc. 2016, 138, 4401−4407

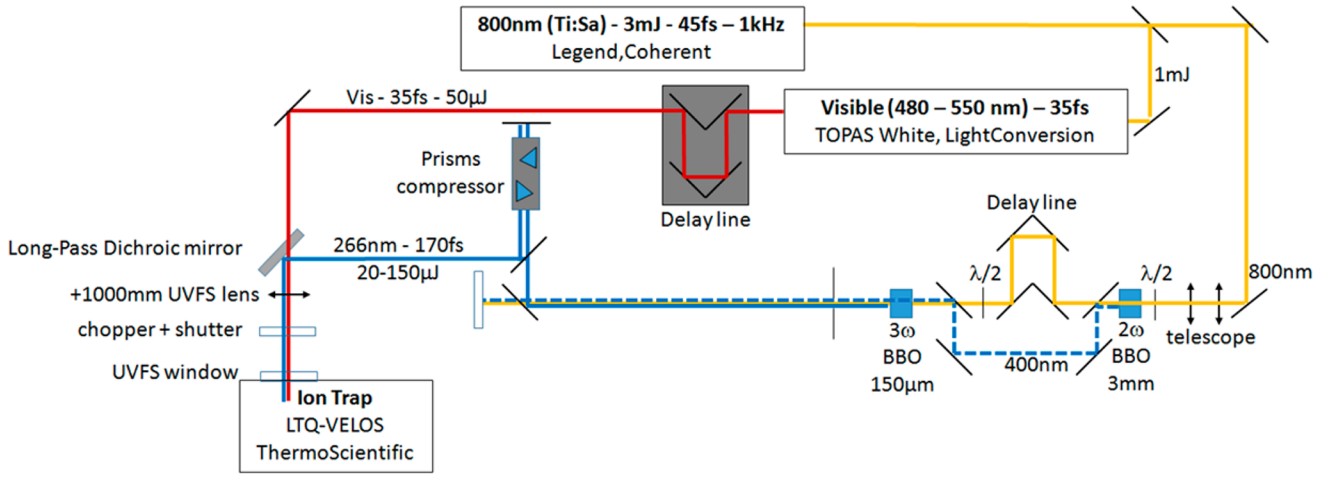


**Figure 6.** Schematic representation of the optical setup used for femtosecond pump−probe experiments.

**Light Sources.** Femtosecond pump−probe experiments (Figure 6): pump and probe pulses are generated from a Ti:Sa amplified chain (Legend, Coherent −800 nm, 3 mJ, 45 fs pulse duration, 1 kHz). The pump at 266 nm is obtained by frequency-tripling the laser fundamental, its pulse duration was estimated to 170 fs by a self-diffraction FROG (Frequency Resolved Optical Gating). The probe at 550 nm is generated by a noncollinear optical parametric amplifier (TopasWhite, Light Conversion) pumped by 1 mJ of the 800 nm laser output.

Nanosecond pump−probe experiments (Figure S5): 266 nm quadrupled output of an Nd:YAG (Brilliant B, Quantel −7 ns pulsewidth, 20 Hz) was used as pump. Energy was lowered to 6 mJ/pulse by delaying the Q-switch with regards to the flash (~400 $\mu$s). Output from an optical parametric oscillator (OPO) in the visible range (PantherEx pumped with Surelite II, Continuum −7 ns pulsewidth, 10 Hz) was used as probe.

Steady state optical spectroscopy experiments: the nanosecond visible OPO output was tuned at selected wavelength between 430 and 630 nm.

**Optical Spectroscopy Protocol.** Solutions of [CuTerpyridine,$HG_3W$]$^{2+}$ ($m/z$ 553) and [CuTerpyridine,$G_3W$]$^{2+}$ ($m/z$ 416) were alternatively electrosprayed, and doubly charged ions of interest were mass selected and dissociated by CID. The radical peptides thus formed were mass selected and trapped for 180 ms. In order to allow a single OPO pulse in the ion trap during this activation time, a microcontroller (Arduino Uno Rev3) was used to trigger the opening of a shutter on the optical path. At the end of the activation time, a mass spectrum is recorded.

The equivalent of the absorption cross section of a given "parent" ion for gas phase action spectroscopy is the fragmentation yield (FY) which is given by Equation 1.

$$\mathrm{FY} = -\log\left(\frac{P}{P+F}\right)/(\lambda\cdot \mathrm{Pw}) \quad (1)$$

Equationwhere $P$ and $F$ are the intensities on the mass spectrum for respectively the parent ion and the ensemble of photofragment ions, and $\lambda$ and Pw are, respectively, the wavelength and average power of the incoming visible laser beam.

**Pump−Probe Experiment Protocol.** Solutions containing silver nitrate and $HG_3W$ peptide were electrosprayed and singly charged [$HG_3W$+Ag]$^+$ ions ($m/z$ 660) were mass selected in the linear ion trap and trapped thereafter in order to let them interact with laser beams and perform pump−probe experiments. Pump and probe beams are recombined and sent collinearly into the mass spectrometer through the fused silica window. Each mass spectrum is recorded after interaction of ions with a single pair of pump and probe pulses.

Ultrafast (fs) pump−probe experiments: Prior to recombination with a dichroic mirror (Semrock FF310_Di01), a microcontrolled delay line (PI M-505 4DG) set on the probe beam path enables to control the optical path with a 1 $\mu$m repeatability, corresponding to 6 fs. The combination of an optical chopper (NewFocus 3501, to reduce effective repetition rate) with a mechanical shutter (Thorlabs SH05, for pulse picking) allows for the injection of a single pump and a single probe pulses in the trap during the activation time. The logic for the synchronization is implemented with a microcontroller (Arduino Uno Rev3). This ensures a single pair of pulses is interacting with parent ions before a mass spectrum is recorded. Electron transfer is monitored via the evolution of silver-containing to silver-free ion intensity ratio as a function of pump−probe delays.

Nanosecond pump−probe experiments: both lasers are triggered externally from a single pulse/delay generator operated at 10 Hz (Stanford Research Systems—DG645). Both beams are directed to a fast photodiode (Thorlabs DET10A, 1 ns rise time), and their respective time width and relative arrival times are characterized from the photodiode profile. Pump−probe delay is electronically adjusted with the delay generator on a nanosecond to millisecond range. A microcontroller (Arduino Uno Rev3) was used to trigger the opening of mechanical shutters (Thorlabs SH05). The two laser beams are recombined with a dichroic mirror (Thorlabs DMLP435). Again, a single pair of pump and probe pulses interacts with ions before a mass spectrum is recorded. Modification of radical peptide's structure is monitored with the evolution of its FY along with pump−probe delays.

**Computational Methods.** All MD simulations were carried out in the gas phase, for both the neutral and protonated peptide, $HG_3W^{\bullet}$ and $HG_3W^{\bullet+}$ respectively, using CHARMM version c40a1.[50] The simulations were started from different initial structures: The first series started from an extended structure of the protonated peptide, the second and the third series were started from two DFT-optimized structures of the [$HG_3W$+Ag]$^+$ complex prior to electron transfer[33] (Figure S7A,D) after removing the silver atom. First, the three initial structures were minimized with 50 000 steps of steepest descent (SD) minimization. This was followed by individual runs with different random seeds which consisted of 30 ps of heating from 0 to 300 K, 250 ps of equilibration dynamics, and 10 ns of production simulations in the gas phase. The equations of motion were propagated with the Verlet algorithm and the time step was $\Delta t$ = 1 fs. Bonds involving hydrogens were constrained with SHAKE.[51] Coordinates were stored every 0.15 ps. For each system, 50 independent simulations were run. For 8 runs starting from structure S7D these simulations were extended to 1 $\mu$s each and coordinates were stored every 1 ns.

All electronic structure calculations were carried out with GAUSSIAN09.[52] In addition to the standard force field for the peptide,[53] a consistent set of atomic charges for the positively charged residue $W^{\bullet+}$ is required for the simulations. These charges were determined at the HF/6-31G(d) level, the same level used to compute and scale charges for the other amino acid residues in the standard force field. For consistency, a new set of atomic charges for neutral $W^{\bullet}$


DOI: 10.1021/jacs.5b12587
J. Am. Chem. Soc. 2016, 138, 4401−4407

and H, as well as deprotonated $W^{\bullet-}$ and protonated $H^+$, was also determined. The histidine protonation state was neutral with the extra hydrogen at N$\delta$. The atomic charges were calculated based on fits to the electrostatic potential (ESP). Charges for $W^{\bullet}$, $W^{\bullet+}$, $W^{\bullet-}$, H, and $H^+$ were extracted from such calculations and a scaling factor between them and the original CHARMM charges were determined. This yields a new set of charges, referred to as CHARMM*, summarized in Tables S1 and S2 for for $W^{\bullet}$, $W^{\bullet+}$, $W^{\bullet-}$, H, and $H^+$ respectively.

Starting from the reactant and product coordinates (Table S3), a transition state with one imaginary frequency was determined from Synchronous Transit-guided Quasi-Newton method.[54,55] Geometries of the initial and the transition states were fully optimized, and vibrational analyses were carried out to confirm the nature of the stationary points ($3n - 6$ real vibrations for reactants and products and one imaginary frequency for the transition states). Free energies were calculated using zero-point vibrational energies (ZPE) and thermal contributions to the Gibbs free energy computed in vacuo. Optimized geometries, frequencies, and free energies of the reactant and the transition state were calculated at the B3LYP/6-31G* level. According to transition state theory (TST) the rate of a gas phase reaction at a given temperature is given by:

$$k(T) = \frac{k_B T}{h} \exp(-\Delta G^{\ddagger}/k_B T)$$

where $\Delta G^{\ddagger} = G^{\ddagger} - G^{\text{react}}$ is the free energy barrier being the difference between the free energy of the transition state and the reactants. For hydrogen/deuterium kinetic isotope effects, the observed values are typically governed by the zero-point energy (ZPE) contribution,[56] and are computed from:

$$\text{KIE} = \frac{k_H}{k_D} = e^{\Delta G_D^{\ddagger} - \Delta G_H^{\ddagger}/RT} = e^{\Delta \text{ZPE}_{GS} - \Delta \text{ZPE}_{TS}/RT}$$

Here, $\Delta \text{ZPE}_{GS}$ and $\Delta \text{ZPE}_{TS}$ are the difference in ZPE between H- and D-containing species in the ground state and the transition state, respectively.

Excited states were calculated at the CAM-B3LYP[57,58]/TZVP[59] level of theory using time-dependent density functional theory (TD)DFT within the unrestricted Kohn–Sham formalism after optimization of the doublet ground state.

## ■ ASSOCIATED CONTENT

### Supporting Information

The Supporting Information is available free of charge on the ACS Publications website at DOI: 10.1021/jacs.5b12587.

Computational details for simulations on $HG_3W^{\bullet+}$ (tables of atomic charges for tryptophan and histidine) and for transition state optimization (coordinates and energies). Mass spectra and fragmentation signature of the metal–peptide cation. Proton transfer time constants evaluated at different wavelengths. Scheme of the nanosecond pump–probe setup. Distribution of indoleNH–inmidazoleN along MD trajectories starting from extended peptide conformations. Compact peptide structures. Decay curves for deuterated/nondeuterated species. NMR $^1$H spectra of the peptide in $D_2O$. TD-DFT optical spectra for different radical position (PDF)

## ■ AUTHOR INFORMATION


### Corresponding Author

*luke.macaleese@univ-lyon1.fr


### Notes

The authors declare no competing financial interest.

## ■ ACKNOWLEDGMENTS

The research leading to these results has received funding from the European Research Council under the European Union's Seventh Framework Program (FP7/2007-2013 Grant agreement N°320659). The Lyon-Geneva collaboration was also supported by the French Ministry of Foreign Affairs (MAE) and Ministry of Education and Research (MESR) via the research funding program "PHC Germaine de Staël" (project N° 30699ZJ). S.H. acknowledges cofunding under FP7-MarieCurie Cofund. K.E.H., M.M., S.H., L.B., and J.P.W. wish to acknowledge the Swiss National Foundation for Research for their support within the NCCR MUST program (200021-117810). Authors wish to acknowledge Michel Moret at Univ. Geneva (CH) for important technical support, and Maggy Hologne at Institut des Sciences Analytiques (Lyon, FR) for NMR data.

## ■ REFERENCES


(1) Hammes-Schiffer, S. *J. Am. Chem. Soc.* **2015**, *137*, 8860.
(2) Migliore, A.; Polizzi, N. F.; Therien, M. J.; Beratan, D. N. *Chem. Rev.* **2014**, *114*, 3381.
(3) Weinberg, D. R.; Gagliardi, C. J.; Hull, J. F.; Murphy, C. F.; Kent, C. A.; Westlake, B. C.; Paul, A.; Ess, D. H.; Granville McCafferty, D.; Meyer, T. J. *Chem. Rev.* **2012**, *112*, 4016.
(4) Zhang, L.; Silva, D.-A.; Zhang, H.; Yue, A.; Yan, Y.; Huang, X. *Nat. Commun.* **2014**, *5*, 4170.
(5) Kaila, V. R. I.; Wikström, M.; Hummer, G. *Proc. Natl. Acad. Sci. U. S. A.* **2014**, *111*, 6988.
(6) Sazanov, L. a. *J. Bioenerg. Biomembr.* **2014**, *46*, 247.
(7) Reece, S. Y.; Seyedsayamdost, M. R.; Stubbe, J.; Nocera, D. G. *J. Am. Chem. Soc.* **2007**, *129*, 8500.
(8) Mulder, D. W.; Ratzloff, M. W.; Bruschi, M.; Greco, C.; Koonce, E.; Peters, J. W.; King, P. W. *J. Am. Chem. Soc.* **2014**, *136*, 15394.
(9) Smirnov, V. V.; Roth, J. P. *JBIC, J. Biol. Inorg. Chem.* **2014**, *19*, 1137.
(10) Nara, S. J.; Valgimigli, L.; Pedulli, G. F.; Pratt, D. a. *J. Am. Chem. Soc.* **2010**, *132*, 863.
(11) Prashanthi, S.; Bangal, P. R. *Chem. Commun.* **2009**, 1757.
(12) Kumar, P. H.; Venkatesh, Y.; Prashanthi, S.; Siva, D.; Ramakrishna, B.; Bangal, P. R. *Phys. Chem. Chem. Phys.* **2014**, *16*, 23173.
(13) Megiatto, J. D., Jr.; Mendez-Hernandez, D. D.; Tejeda-Ferrari, M. E.; Teillout, A.-L.; Llansola-Portoles, M. J.; Kodis, G.; Poluektov, O. G.; Rajh, T.; Mujica, V.; Groy, T. L.; Gust, D.; Moore, T. A.; Moore, A. L. *Nat. Chem.* **2014**, *6*, 423.
(14) Oltrogge, L. M.; Wang, Q.; Boxer, S. G. *Biochemistry* **2014**, *53*, 5974.
(15) Meyer, T. J.; Huynh, M. H. V; Thorp, H. H. *Angew. Chem., Int. Ed.* **2007**, *46*, 5284.
(16) Irebo, T.; Reece, S. Y.; Sjödin, M.; Nocera, D. G.; Hammarström, L. *J. Am. Chem. Soc.* **2007**, *129*, 15462.
(17) Hodgkiss, J. M.; Damrauer, N. H.; Pressé, S.; Rosenthal, J.; Nocera, D. G. *J. Phys. Chem. B* **2006**, *110*, 18853.
(18) Warren, M. M.; Kaucikas, M.; Fitzpatrick, A.; Champion, P.; Sage, J. T.; van Thor, J. J. *Nat. Commun.* **2013**, *4*, 1461.
(19) Hodgkiss, J. M.; Krivokapić, A.; Nocera, D. G. *J. Phys. Chem. B* **2007**, *111*, 8258.
(20) Du, R.; Liu, C.; Zhao, Y.; Pei, K.-M.; Wang, H.-G.; Zheng, X.; Li, M.; Xue, J.-D.; Phillips, D. L. *J. Phys. Chem. B* **2011**, *115*, 8266.
(21) Fang, C.; Frontiera, R. R.; Tran, R.; Mathies, R. a. *Nature* **2009**, *462*, 200.
(22) Guyon, L.; Tabarin, T.; Thuillier, B.; Antoine, R.; Broyer, M.; Boutou, V.; Wolf, J.-P.; Dugourd, P. *J. Chem. Phys.* **2008**, *128*, 75103.
(23) Reitsma, G.; Gonzalez-Magaña, O.; Versolato, O.; Door, M.; Hoekstra, R.; Suraud, E.; Fischer, B.; Camus, N.; Kremer, M.; Moshammer, R.; Schlathölter, T. *Int. J. Mass Spectrom.* **2014**, *365–366*, 365.




DOI: 10.1021/jacs.5b12587
*J. Am. Chem. Soc.* 2016, 138, 4401–4407

(24) Nolting, D.; Schultz, T.; Hertel, I. V.; Weinkauf, R. *Phys. Chem. Chem. Phys.* **2006**, *8*, 5247.
(25) Nolting, D.; Weinkauf, R.; Hertel, I. V.; Schultz, T. *ChemPhysChem* **2007**, *8*, 751.
(26) Soorkia, S.; Broquier, M.; Grégoire, G. *J. Phys. Chem. Lett.* **2014**, *5*, 4349.
(27) Chatterley, A. S.; West, C. W.; Stavros, V. G.; Verlet, J. R. R. *Chem. Sci.* **2014**, *5*, 3963.
(28) Støchkel, K.; Wyer, J. A.; Kirketerp, M. B. S.; Brøndsted Nielsen, S. *J. Am. Soc. Mass Spectrom.* **2010**, *21*, 1884.
(29) Bagheri-Majdi, E.; Ke, Y.; Orlova, G.; Chu, I. K.; Hopkinson, A. C.; Siu, K. W. M. *J. Phys. Chem. B* **2004**, *108*, 11170.
(30) Hopkinson, A. C.; Siu, K. W. M. In *Principles of Mass Spectrometry Applied to Biomolecules*; Laskin, J., Lifshitz, C., Eds.; John Wiley & Sons, Inc.: Hoboken, NJ, USA, 2006.
(31) Barlow, C. K.; McFadyen, W. D.; O'Hair, R. A. J. *J. Am. Chem. Soc.* **2005**, *127*, 6109.
(32) Bellina, B.; Compagnon, I.; Houver, S.; Maître, P.; Allouche, A.-R.; Antoine, R.; Dugourd, P. *Angew. Chem., Int. Ed.* **2011**, *50*, 11430.
(33) Bellina, B.; Compagnon, I.; MacAleese, L.; Chirot, F.; Lemoine, J.; Maître, P.; Broyer, M.; Antoine, R.; Kulesza, A.; Mitrić, R.; Bonačić-Koutecký, V.; Dugourd, P. *Phys. Chem. Chem. Phys.* **2012**, *14*, 11433.
(34) Joly, L.; Antoine, R.; Allouche, A.-R.; Dugourd, P. *J. Am. Chem. Soc.* **2008**, *130*, 13832.
(35) Harrison, A. G. *Mass Spectrom. Rev.* **1997**, *16*, 201.
(36) Siu, C. K.; Ke, Y.; Orlova, G.; Hopkinson, A. C.; Michael Siu, K. W. *J. Am. Soc. Mass Spectrom.* **2008**, *19*, 1799.
(37) Sobolewski, A. L.; Domcke, W.; Dedonder-Lardeux, C.; Jouvet, C. *Phys. Chem. Chem. Phys.* **2002**, *4*, 1093.
(38) Grégoire, G.; Jouvet, C.; Dedonder-Lardeux, C.; Sobolewski, A. L. *J. Am. Chem. Soc.* **2007**, *129*, 6223.
(39) Boyarkin, O. V.; Mercier, S. R.; Kamariotis, A.; Rizzo, T. R. *J. Am. Chem. Soc.* **2006**, *128*, 2816.
(40) Kang, H.; Dedonder-Lardeux, C.; Jouvet, C.; Grégoire, G.; Desfrançois, C.; Schermann, J. P.; Barat, M.; Fayeton, J. A. *J. Phys. Chem. A* **2005**, *109*, 2417.
(41) Berdakin, M.; Féraud, G.; Dedonder-Lardeux, C.; Jouvet, C.; Pino, G. a. *J. Phys. Chem. Lett.* **2014**, *5*, 2295.
(42) Goerigk, L.; Grimme, S. *J. Chem. Theory Comput.* **2010**, *6*, 107.
(43) Krishtalik, L. I. *Biochim. Biophys. Acta, Bioenerg.* **2000**, *1458*, 6.
(44) Gil, H.; Mata-Segreda, J. F.; Schowen, R. L. *J. Am. Chem. Soc.* **1988**, *110*, 8265.
(45) Kwon, O.-H.; Zewail, A. H. *Proc. Natl. Acad. Sci. U. S. A.* **2007**, *104*, 8703.
(46) Fita, P.; Urbanska, N.; Radzewicz, C.; Waluk, J. *Chem. - Eur. J.* **2009**, *15*, 4851.
(47) Roubelakis, M. M.; Bediako, D. K.; Dogutan, D. K.; Nocera, D. G. *Energy Environ. Sci.* **2012**, *5*, 7737.
(48) Saxena, A. M.; Udgaonkar, J. B.; Krishnamoorthy, G. *Protein Sci.* **2005**, *14*, 1787.
(49) Sant'Ana, a. C.; Alves, W. a.; Santos, R. H. a; Ferreira, a. M. D.; Temperini, M. L. a. *Polyhedron* **2003**, *22*, 1673.
(50) Brooks, B. R.; Brooks, C. L., III; Mackerell, A. D., Jr.; Nilsson, L.; Petrella, R. J.; Roux, B.; Won, Y.; Archontis, G.; Bartels, C.; Boresch, S.; Caflisch, A.; Caves, L.; Cui, Q.; Dinner, A. R.; Feig, M.; Fischer, S.; Gao, J.; Hodoscek, M.; Im, W.; Kuczera, K.; Lazaridis, T.; Ma, J.; Ovchinnikov, V.; Paci, E.; Pastor, R. W.; Post, C. B.; Pu, J. Z.; Schaefer, M.; Tidor, B.; Venable, R. M.; Woodcock, H. L.; Wu, X.; Yang, W.; York, D. M.; Karplus, M. *J. Comput. Chem.* **2009**, *30*, 1545.
(51) van Gunsteren, W. F.; Berendsen, H. J. C. *Mol. Phys.* **1977**, *34*, 1311.
(52) Frisch, M. J.; Trucks, G. W.; Schlegel, H. B.; Scuseria, G. E.; Robb, M. A.; Cheeseman, J. R.; Scalmani, G.; Barone, V.; Mennucci, B.; Petersson, G. A.; Nakatsuji, H.; Caricato, M.; Li, X.; Hratchian, H. P.; Izmaylov, A. F.; Bloino, J.; Zheng, G.; Sonnenberg, J. L.; Hada, M.; Ehara, M.; Toyota, K.; Fukuda, R.; Hasegawa, J.; Ishida, M.; Nakajima, T.; Honda, Y.; Kitao, O.; Nakai, H.; Vreven, T.; Montgomery Jr., J. A.; Peralta, J. E.; Ogliaro, F.; Bearpark, M.; Heyd, J. J.; Brothers, E.; Kudin, K. N.; Staroverov, V. N.; Kobayashi, R.; Normand, J.; Raghavachari, K.; Rendell, A.; Burant, J. C.; Iyengar, S. S.; Tomasi, J.; Cossi, M.; Rega, N.; Millam, J. M.; Klene, M.; Knox, J. E.; Cross, J. B.; Bakken, V.; Adamo, C.; Jaramillo, J.; Gomperts, R.; Stratmann, R. E.; Yazyev, O.; Austin, A. J.; Cammi, R.; Pomelli, C.; Ochterski, J. W.; Martin, R. L.; Morokuma, K.; Zakrzewski, V. G.; Voth, G. A.; Salvador, P.; Dannenberg, J. J.; Dapprich, S.; Daniels, A. D.; Farkas, Ö.; Foresman, J. B.; Ortiz, J. V; Cioslowski, J.; Fox, D. J. *Gaussian 09*, Revision D.01; Gaussian Inc.: Wallingford CT, 2009.
(53) Mackerell, A. D., Jr.; Bashford, D.; Bellott, M.; Dunbrack, R. L. J.; Evanseck, J. D.; Field, M. J.; Fischer, S.; Gao, J.; Guo, H.; Ha, S.; Joseph-McCarthy, D.; Kuchnir, L.; Kuczera, K.; Lau, F. T. K.; Mattos, C.; Michnick, S.; Ngo, T.; Nguyen, D. T.; Prodhom, B.; Reiher, W. E. I. I. I.; Roux, B.; Schlenkrich, M.; Smith, J. C.; Stote, R.; Straub, J.; Watanabe, M.; Wiorkiewicz-Kuczera, J.; Yin, D.; Karplus, M. *J. Phys. Chem. B* **1998**, *102*, 3586.
(54) Peng, C.; Schlegel, H. B. *Isr. J. Chem.* **1993**, *33*, 449.
(55) Peng, C.; Ayala, P. Y.; Schlegel, H. B.; Frisch, M. J. *J. Comput. Chem.* **1996**, *17*, 49.
(56) Buncel, E.; Lee, C. C. *Isotopes in Organic Chemistry*; Elsevier: Amsterdam, 1977; Vol. 5.
(57) Yanai, T.; Tew, D. P.; Handy, N. C. *Chem. Phys. Lett.* **2004**, *393*, 51.
(58) Becke, A. *J. Chem. Phys.* **1993**, *98*, 5648.
(59) Weigend, F.; Ahlrichs, R. *Phys. Chem. Chem. Phys.* **2005**, *7*, 3297.


DOI: 10.1021/jacs.5b12587
*J. Am. Chem. Soc.* 2016, 138, 4401−4407